AUTHOR(S)
Yu, A., Zhang, W., Zhang, Q., Yang, K., Liu, X., Liu, H., Xie, J., Feng, Y., Li, J. & Jia, C.

TITLE
A TICT-AIE activated dual-channel fluorescence-on probe to reveal the dynamics mechanosensing of lipid droplets during ferroptosis

YEAR
2024

DOI
10.1016/j.talanta.2024.126028

CITATION
Yu, A., Zhang, W., Zhang, Q., Yang, K., Liu, X., Liu, H., Xie, J., Feng, Y., Li, J., & Jia, C. (2024). A TICT-AIE activated dual-channel fluorescence-on probe to reveal the dynamics mechanosensing of lipid droplets during ferroptosis. *Talanta, 274*, 126028. https://doi.org/10.1016/j.talanta.2024.126028

VERSION
Accepted Manuscript

A TICT-AIE activated dual-channel fluorescence-on probe to reveal the dynamics mechanosensing of lipid droplets during ferroptosis

Ao Yu [a †], Wei Zhang [b †], Qiangsheng Zhang [a], Kunlong Yang [a], Xiongbo Liu [a], Hongtao Liu [a d], Jialin Xie [a d], Yan Feng [a d*], Jianwei Li [c*], Chunman Jia [a d e*]

[a] *Hainan Provincial Key Laboratory of Fine Chem, School of chemistry and chemical engineering, Hainan University, Haikou 570228, China.*

[b] *Key Laboratory of Hainan Trauma and Disaster Rescue, The First Affiliated Hospital of Hainan Medical University, Hainan Medical University, Haikou, 571199 P. R. China*

[c] *MediCity Research Laboratory, University of Turku, Tykistökatu 6, Turku, 20520, Finland*

[d] *One Health Institute, Hainan University, Haikou, 570228, China*

[e] *Analytical & Testing Center, Hainan University, Haikou, 570228, China*

[†] Ao Yu and Wei Zhang contributed equally to this work and should be regarded as co-first authors.

Abstract

Mechanical forces play a crucial role in cellular processes, including ferroptosis, a form of regulated cell death associated with various diseases. However, the mechanical aspects of organelle lipid droplets (LDs) during ferroptosis are poorly understood. In this study, we designed and synthesized a fluorescent probe, **TPE-V1**, to enable real-time monitoring of LDs' viscosity using a dual-channel fluorescence-on model (red channel at 617 nm and NIR channel at 710 nm). The fluorescent imaging of using **TPE-V1** was achieved due to the integrated mechanisms of the twisted intramolecular charge transfer (TICT) and aggregation-induced emission (AIE). Through dual-emission channel fluorescence imaging, we observed the enhanced mechanical energy of LDs triggering cellular mechanosensing, including ferroptosis

* Corresponding author: E-mail address: fengy@hainanu.edu.cn
* Corresponding author: E-mail address: jianwei.li@utu.fi
* Corresponding author: E-mail address: jiachunman@hainanu.edu.cn

and cell deformation. Theoretical calculations confirmed the probe's behavior, showing that high-viscosity media prevented the rotation processes and restored fluorescence quenching in low viscosity. These findings suggest that our TICT-TPE design strategy provides a practical approach to study LDs' mechanical properties during ferroptosis. This development enhances our understanding of the interplay between mechanical forces and LDs, contributing to the knowledge of ferroptotic cell death and potential therapeutic interventions targeting dysregulated cell death processes.

Keywords: TICT-AIE; dual-channel; lipid droplets; mechanosensing; ferroptosis

1. Introduction

Cellular processes are intricately regulated by a complex interplay of biochemical signaling and physical forces [1]. Recent research has revealed the profound impact of mechanical forces, including mechano-sensing and mechano-transduction, on diverse cellular functions [2, 3]. These processes involve the detection and conversion of mechanical signals into biochemical responses, influencing critical cellular phenomena such as cell growth, differentiation, and cell death [4-7]. Ferroptosis, a novel form of regulated cell death [8], has gained significant attention due to its involvement in various pathological conditions, ranging from cancer to neurodegenerative diseases and tissue damage [9-11]. This unique form of cell death is characterized by the accumulation of reactive oxygen species (ROS) and lipid peroxides [12-16], resulting in cellular dysfunction and demise. While the biochemical aspects of ferroptosis have been extensively studied, the role of mechanical forces, particularly their impact on the organelles involved, remains largely unexplored. Among the organelles implicated in ferroptosis, organelle lipid droplets (LDs) have recently come under intense scrutiny. Once considered passive lipid storage depots, LDs are now recognized as dynamic organelles with multifaceted functions, including lipid metabolism, energy homeostasis, and cellular signaling [17-21]. Given their involvement in lipid metabolism, LDs are poised to play a critical role in mediating cellular responses to mechanical forces during ferroptosis.

However, the investigation of mechanical forces, specifically the influence of viscosity, on organelle LDs poses a substantial challenge, with the lack of practical methodologies hindering progress in this area. Notably, intracellular viscosity is a key mechanical force (fluid shear stress), and viscosity has a numerical relationship with shear stress per unit velocity gradient [22]. In this study, to address this pressing need, we propose to design probe molecules that can sense the change of LDs' mechanical properties during ferroptosis through fluorescence imaging under the integrated mechanisms of both TICT and AIE. This should provide a pioneering and practical approach to explore the mechanical aspects of LDs during ferroptosis.

Fluorescence imaging has emerged as a powerful tool for monitoring the cellular microenvironment, offering high sensitivity, real-time capabilities, non-invasiveness, and in situ visual imaging [23-26]. Existing fluorescent probes for tracking LDs' mechanical force changes often suffer from limitations such as aggregation-induced quenching (ACQ) effects [27-29], low dosages, and poor emission in bioassays. Furthermore, some probes typically exhibit visible fluorescence with single-wavelength emission [30, 31], making them susceptible to background fluorescence interference. In contrast, fluorescence qualitative analysis using single-wavelength excitation and dual-emission channels offers improved data accuracy and simplified operational procedures, benefiting from built-in self-calibration mechanisms [32, 33]. Additionally, probes with red and near-infrared (NIR) fluorescence emission hold advantages in fluorescence bioimaging, including reduced autofluorescence of biomolecules, reduced photobleaching, and enhanced tissue penetration capabilities [34, 35].

Therefore, there is a critical need to develop probes for real-time monitoring of LDs' viscosity through single-excitation and dual-emission channels with red and NIR fluorescence. In recent studies, probes based on intramolecular motion mechanisms (RIM) [36-40] or TICT phenomenon [41-45] have been used to monitor the viscosity of LDs in real time. Meanwhile, according to reports, probes with TICT and AIE mechanisms (also known as TICT-AIE) exhibit tunable emission characteristics [46-

48], with increased TICT effects causing red-shifted fluorescence emission [49, 50]. This property allows TICT-AIE probes to display distinct optical characteristics in different fluorescence emission channels. However, until now, there has been no examples of integrating TICT and AIE into a single probe to detect the viscosity changes of LDs. On the basis of this, we anticipate that TICT-AIE probes will be able to dynamically realize accurately tracking the viscosity changes of LDs in dual emission channels.

Here, we present the design of the first TICT-AIE integrated probe, **TPE-V1**, specifically for tracking LDs' mechanical property changes during ferroptosis through red and NIR emission channels. **TPE-V1** incorporates merocyanine, cyclohexene, and TPE moieties. The extended π-conjugated system with enhanced rigidity enables the molecule to exhibit NIR emission, while the bonds between merocyanine and cyclohexene act as a molecular rotor that freely rotates in low-viscosity solvents, rendering the probe sensitive to viscosity changes. Additionally, TPE, as an AIE-active core and a viscosity-sensitive unit, selectively accumulates in LDs due to its hydrophobicity. Based on the TICT-AIE mechanism, bond rotation in the merocyanine and TPE molecules is restricted under viscous media, leading to enhanced fluorescence intensity in both emission channels. Theoretical calculations further validate the probe's behavior, demonstrating that a high-viscosity medium prevents the TICT and AIE rotation processes of the probe. Moreover, **TPE-V1** exhibits high specificity and low cytotoxicity. With its unique advantages, **TPE-V1** serves as an excellent fluorescence sensor for dynamically monitoring the mechanical force of LDs through two different emission channels. This development significantly advances the in-depth study of LDs' mechanosensing during ferroptosis and paves the way for further exploration of the complex interplay between mechanical forces and LDs, fostering a deeper understanding of ferroptotic cell death and opening new possibilities for therapeutic interventions targeting dysregulated cell death processes.

2. Experimental section

2.1 Materials and general experimental methods

For detailed information, please refer to the Supporting Information. The synthesis of **TPE-V1** involved stirring a solution of **4** (150 mg, 0.38 mmol), **1** (180 mg, 0.48 mmol), and KOH (304 mg, 5.42 mmol) in ethanol (12 mL) at room temperature. Subsequently, five drops of tributyl ammonium hydroxide solution (0.8 M) were added, and the mixture was heated to reflux for 5 hours. The progress of the reaction was monitored using TLC. After cooling to room temperature, the solution was concentrated under reduced pressure. The crude product was purified by column chromatography using PE/CH_2Cl_2 (20:1) as the eluent, resulting in the isolation of probe **TPE-V1** compound (150 mg, 53% yield) as a green solid. ^{1}H NMR (400 MHz, $CDCl_3$) analysis showed the following values: δ 8.02 (d, J = 8.7 Hz, 2H), 7.81 (d, J = 8.2 Hz, 1H), 7.77 (d, J = 8.7 Hz, 1H), 7.49 - 7.43 (m, 1H), 7.39 (s, 2H), 7.17 - 7.00 (m, 21H), 3.84 (s, 2H), 3.04 (s, 2H), 2.61 (s, 2H), 1.97 (s, 6H), 1.89 (s, 2H), 1.32 (d, J = 8.0 Hz, 3H). ^{13}C NMR (100 MHz, $CDCl_3$) analysis yielded the following values: δ 143.60, 143.49, 139.29, 131.87, 131.39, 130.97, 129.85, 129.25, 127.88, 127.73, 127.64, 126.74, 126.59, 126.52, 124.76, 122.87, 121.63, 109.51, 49.61, 40.89, 27.02, 22.66, 21.26, 21.06, 12.98. MS (ESI) m/z for $([C53H45ClN2]+H)^+$: calculated: 745.3350, observed: 745.3356 (Scheme S1, Figures S1-S7).

2.2 Measurement of fluorescence lifetime

The fluorescence lifetime of **TPE-V1** was recorded using a HORIBA Fluorolog-3 instrument with NanoLED, λex=540 nm. Further experimental details are provided in the Supporting Information.

2.3 DFT calculations

The ground-state structures of **TPE-V1** were optimized using Gaussian 09 software based on CAM-B3LYP-GD3/6-311G**. The excited state-related calculations of **TPE-V1** and **TPE-V2** were performed using time-dependent density functional theory (TD-DFT) with the optimized structure of the ground state.

2.4 Cell imaging experiment

To monitor the response of LDs' viscosity, the control group was treated with **TPE-V1** (20 μM) for 10 minutes and subsequently treated with PBS (10 μM) for 30 minutes. In the experimental group, HeLa cells were treated with **TPE-V1** (20 μM) for 10 minutes and then treated with nystatin, which induces an increase in intracellular viscosity, for an additional 30 minutes. After being washed three times with PBS, fluorescence imaging was performed using a confocal laser scanning microscope (OLYMPUS FV3000). The fluorescence emission was collected in the red channel (580-630 nm) and NIR channel (650-750 nm) with an excitation wavelength of 560 nm.

2.5 Imaging of LDs viscosity during ferroptosis

For imaging the viscosity of LDs during ferroptosis, living HeLa cells were treated with 20 μM **TPE-V1** for 10 minutes and then incubated with 10 μM erastin (a ferroptosis inducer) or 10 μM erastin and 15 μM Fer-1 (an inhibitor of ferroptosis) for various durations (0-2 hours).

3. Results and discussion

3.1 Design of TPE-V1 for LDs viscosity

In general, increasing structural rigidity has been shown to enhance photostability and quantum yield [51, 52]. Additionally, the incorporation of benzene rings into terminal groups can induce a red-shift in absorption and emission wavelengths [51]. Our design strategy, illustrated in Scheme 1, capitalizes on these principles. By introducing rigid cyclohexene substituents, we aimed to significantly improve the quantum yield and photostability of the probe by reducing nonradiative transitions. Furthermore, the inclusion of multiple aromatic rings promotes a red-shift in fluorescence emission.

To enable reliable viscosity detection, we incorporated two additional rotors (merocyanine and TPE) into the probe. These rotors facilitate free rotation of the bonds, resulting in weak optical signals and short fluorescence lifetimes in low-viscosity solutions. Conversely, in high-viscosity environments, the rotation of these bonds becomes restricted, leading to a significant enhancement in red and NIR fluorescence

signals in the dual-channel detection.

Moreover, the hydrophobic nature of TPE [53] allows **TPE-V1** to selectively aggregate in LDs, becoming embedded in their anhydrous core through strong hydrophobic interactions. As a result, **TPE-V1** serves as a suitable tool for monitoring LDs' viscosity changes based on the TICT-AIE mechanisms, offering detection capabilities in different emission channels.

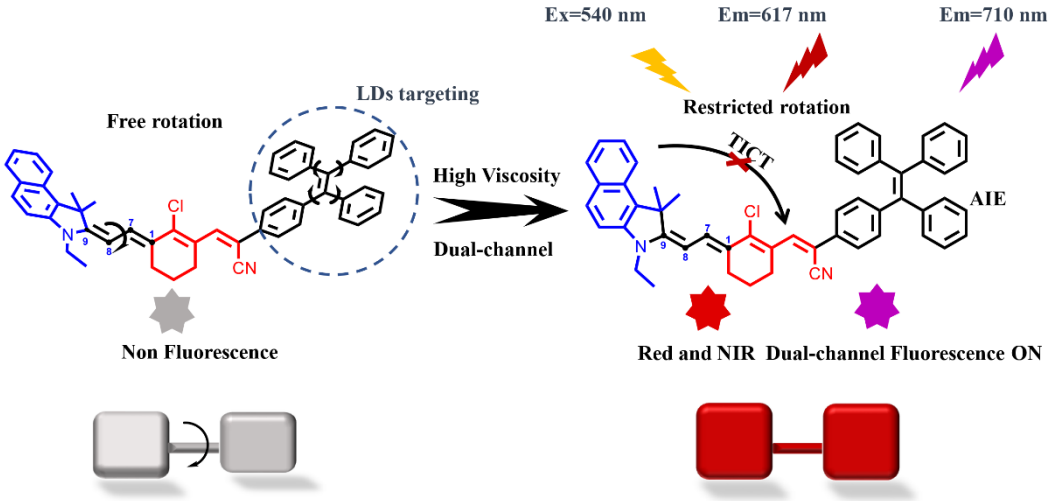

Scheme 1. The schematic diagram of dual-channel visualization viscosity of LDs.

3.2 Theoretical calculation

To gain further insight into the impact of viscosity on the probe's fluorescence at the molecular level, theoretical calculations were employed to investigate the underlying mechanism. As illustrated in Figure 1A, the molecular orbital density analysis reveals strong charge transfer (ICT) from the electron donor (primarily located on the merocyanine moiety) to the electron acceptor (primarily located on the cyclohexene moiety). Furthermore, the C9-C8-C7-C1 bond exhibits free rotation in low-viscosity environments. In the excited state, when the dihedral angle at C9-C8-C7-C1 is approximately 180°, **TPE-V1** adopts a planar conformation, resulting in a locally excited (LE) state with an oscillator strength (fem) of 2.5373. Conversely, when the dihedral angle is 90°, **TPE-V1** adopts an orthogonal conformation, leading to a twisted intramolecular charge transfer (TICT) state with a significantly reduced oscillator

strength (fem) of only 0.0339. This demonstrates that the distinct TICT effect is responsible for the fluorescence quenching observed in the TICT state (Figure 1B).

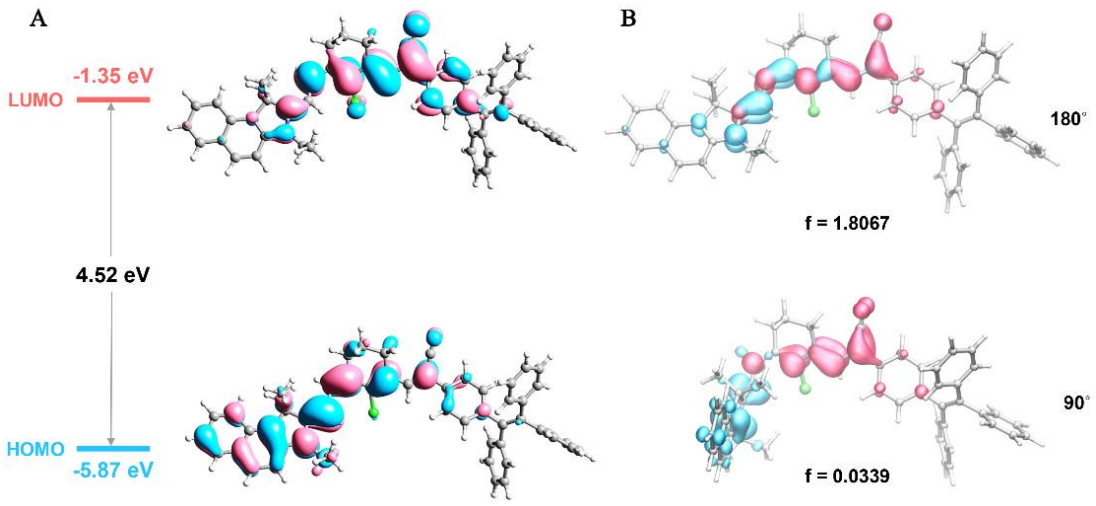

Figure 1. (A) DFT calculation result of **TPE-V1**: energy gap, HOMO, and LUMO. (B) The hole-electron distribution diagram of **TPE-V1** in excited LE and TICT state.

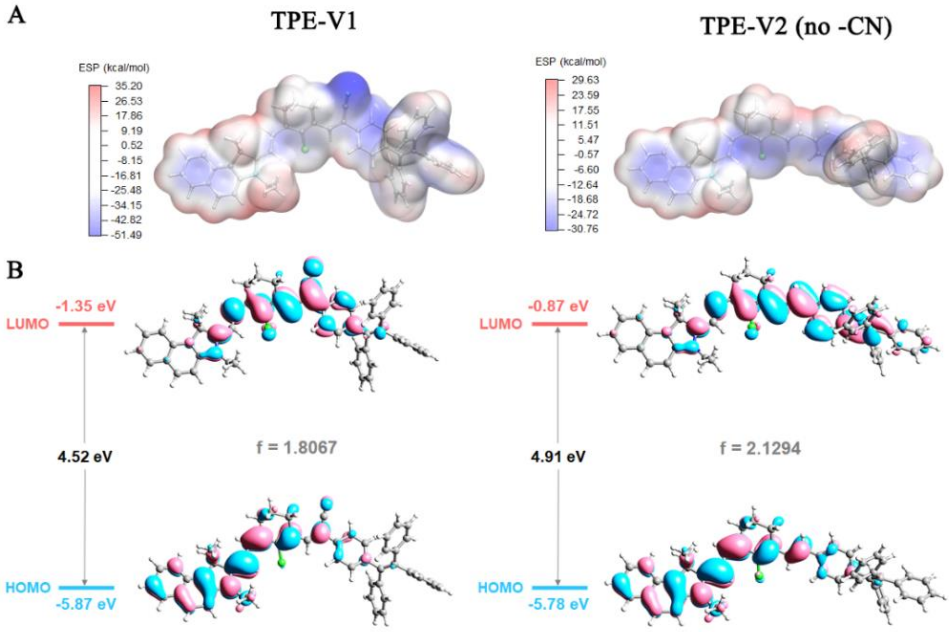

Figure 2. (A) Electrostatic potential (ESP) profile of **TPE-V1** and **TPE-V2 (no-CN)**. (B) HOMO-LUMO distribution, energy gap, calculated **TPE-V1** and **TPE-V2 (no-CN)** by TD-DFT.

Additionally, the TPE group in **TPE-V1** is optimized to exhibit a highly distorted configuration, which facilitates active intramolecular rotations, resulting in aggregation-induced emission (AIE) properties and viscosity responsiveness. The

incorporation of the -CN group, with its strong electron-absorbing ability, generates a polar negative region and reduces the HOMO-LUMO energy gap in **TPE-V1**. As a result, the fluorescence of **TPE-V1** is quenched, as supported by TD-DFT calculations (Figure 2). Therefore, it is reasonable to propose that the viscosity properties of **TPE-V1** are influenced by a synergistic interplay between the TICT and AIE mechanisms.

3.3 AIE properties of TPE-V1

To investigate the aggregation-induced emission (AIE) properties of **TPE-V1**, characterization experiments were conducted in a mixture of DMSO (a good solvent) and water (a poor solvent). Different solutions of the probe were prepared with varying water ratios (F_w=0-99%). As depicted in Figure 3A, **TPE-V1** exhibited an absorption peak at around 578 nm in pure DMSO. As the proportion of water increased to 90%, the UV absorption intensity of **TPE-V1** decreased, accompanied by a slight blue shift to 540 nm. This observation can be attributed to the formation of aggregates as water content increases. The resulting scattering effect causes a reduction in UV absorption intensity.

Furthermore, fluorescence spectra of **TPE-V1** were recorded with excitation at 540 nm. In pure DMSO, **TPE-V1** emitted weak near-infrared (NIR) fluorescence at around 720 nm. Upon the addition of water up to 40%, the emission intensity increased, and a blue-shift of approximately 20 nm was observed. These findings provide further evidence of aggregate formation by **TPE-V1**. However, as the water content of the system continued to reach 90%, the emission intensity at 720 nm decreased (Figure 3B). This may be attributed to the formation of H-aggregates by the probe molecules as the water content increases, resulting in a decrease in fluorescence intensity and even fluorescence quenching [54-55]. Moreover, in highly polar aqueous solutions, there is a competitive relationship between AIE and TICT mechanisms [56-57]. **TPE-V1** has a longer conjugated chain and the indole part of the probe is prone to rotation and the formation of a twisted structure in low viscosity environments. This propensity for twisting intramolecular charge transfer further contributes to the decrease in fluorescence intensity.

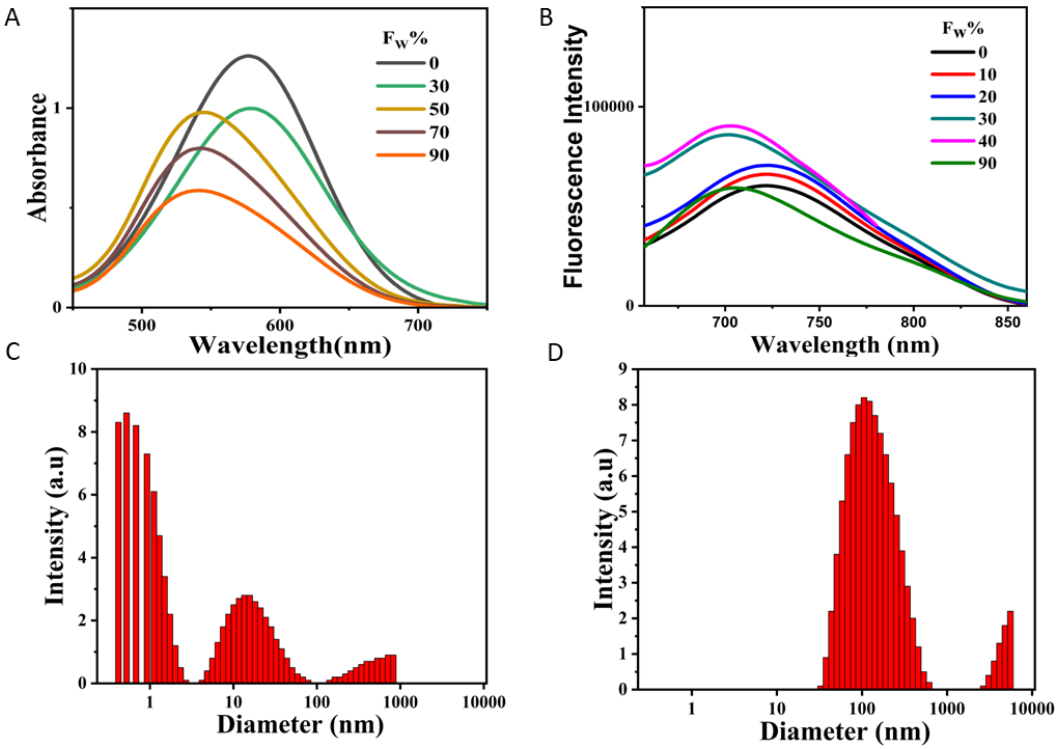

Figure 3. (A) Absorption spectra of **TPE-V1** (10 μM) in the mixture of DMSO and water. (B) Emission spectra of **TPE-V1** (10 μM) in the mixture of DMSO and water, λ_{ex}=540 nm. Particle size distributions of **TPE-V1** (10 μM) in mixed solutions with different proportions of water and DMSO. (C) F_w=20%, (D) F_w=100%.

Additionally, dynamic light scattering (DLS) measurements were employed to detect the aggregation behavior of the AIE fluorogens (Figure S8, Figure 3C and 3D). The results revealed average diameter sizes of approximately 28 nm in DMSO and 145 nm in water, respectively. These findings substantiate the excellent AIE properties exhibited by **TPE-V1**.

3.4 Optical properties and fluorescent lifetime measurement of TPE-V1

To assess the optical properties of **TPE-V1** in relation to viscosity, we examined its performance by mixing varying volume fractions of glycerol with water. As shown in Figure 4A, **TPE-V1** exhibited maximum absorption at 540 nm in pure water. The absorption intensity at 540 nm increased as viscosity transitioned from low (water) to high (glycerol) values.

Under 540 nm excitation, **TPE-V1** emitted weak near-infrared (NIR) fluorescence at 710 nm in low-viscosity solutions. This emission arose from the unrestricted rotation

of the merocyanine and TPE skeleton, resulting in non-radiative decay of the excited state. As viscosity increased from 2.4 cP (0% glycerol) to 360.9 cP (90% glycerol), enhanced emission peaks at 617 nm emerged, indicating the involvement of twisted intramolecular charge transfer (TICT) processes. The charge separation between the donor (D) and acceptor (A) entities was induced under these conditions. Additionally, the rotational freedom of TPE became restricted, leading to the emergence of aggregation-induced emission (AIE) behavior, which manifested as an increased emission peak at 710 nm (Figure 4B). Thus, a combination of TICT and AIE processes was observed, corroborating our proposed mechanism.

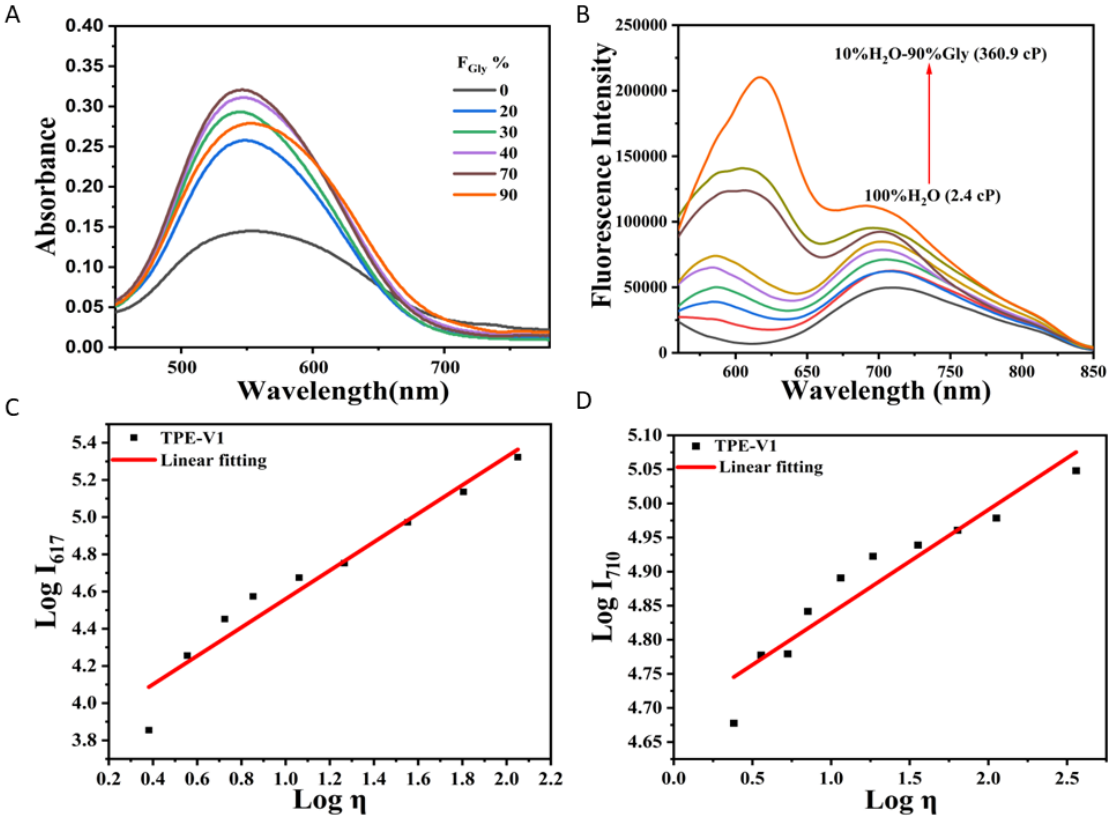

Figure 4. (A) Absorption spectra of **TPE-V1** (10 μM) in solvents of different viscosities. (B) Emission spectra of **TPE-V1** (10 μM) in solvents of different viscosities. (C) The linear relationship between $LogI_{617}$ and Logη, R^2=0.9406. (D) the linear relationship between $LogI_{710}$ and Logη, R^2=0.9027. All fluorescence spectra were acquired at λ_{ex}=540 nm.

Furthermore, a strong linear relationship was observed between $LogI_{617}$ and Logη, as well as between $LogI_{710}$ and Logη, as calculated using the Förster-Hoffmann

equation (see Supporting Information) (Figure 4C and 4D). This suggests that **TPE-V1** holds significant potential for in vivo cellular viscosity detection through various channels. In addition to the enhanced fluorescence intensity, the fluorescence lifetime of **TPE-V1** gradually increased with increasing solvent viscosity. The lifetime of **TPE-V1** lengthened from 5.56 ns to 13.5 ns as the viscosity changed from pure water to 90% glycerol. The linear equation $\log\tau = 0.2690\log\eta + 0.6214$, with a linear coefficient of 0.8752, demonstrated the correlation between lifetime and viscosity (Figure 5). This observation aligns with the enhanced emission intensity observed in solutions with high viscosity. Thus, the fluorescence lifetime serves as another valuable parameter, indicating the sensitivity of **TPE-V1** to viscosity changes.

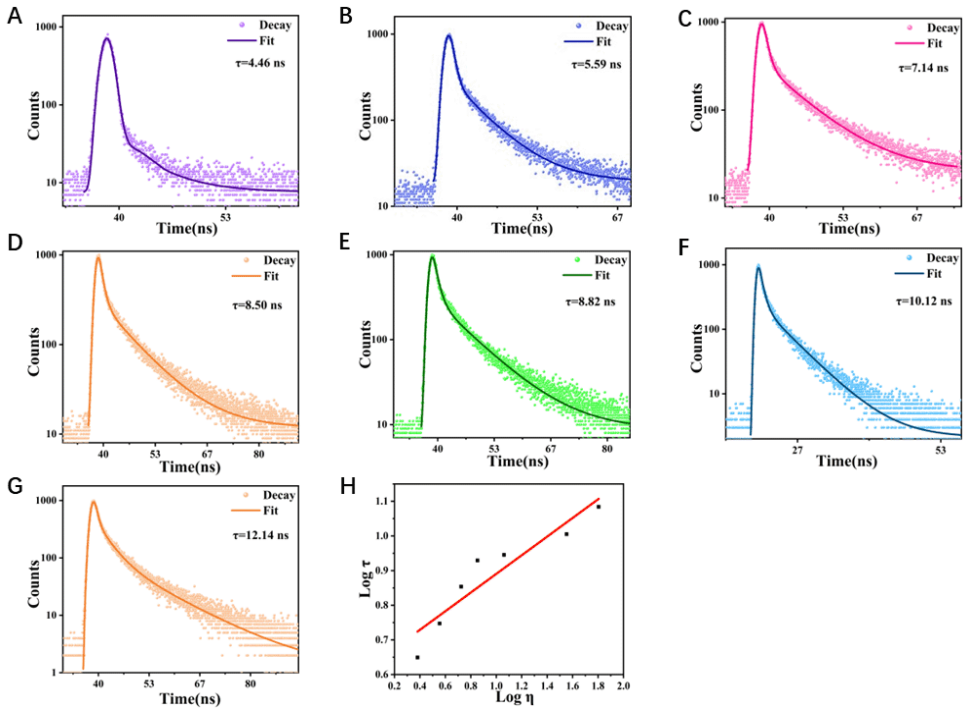

Figure 5. Fluorescence lifetime decay curve of **TPE-V1** in different proportions of glycerol and water. (A) 100% H_2O. (B) 90% H_2O/10% Gly. (C) 80% H_2O/20% Gly. (D) 70% H_2O/30% Gly. (E) 60% H_2O/40% Gly. (F) 40% H_2O/60% Gly. (G) 20% H_2O/80% Gly. (H) the linear relationship between Logτ and Logη.

3.5 Interference resistance of TPE-V1

In the cellular microenvironment, pH is a critical parameter that can potentially interfere with the viscosity detection by the probe. To assess the stability of **TPE-V1** in different pH conditions (ranging from 2 to 12), pH experiments were conducted at both

high and low viscosities. Although the fluorescence intensity of **TPE-V1** exhibited variations at different pH values under high and low viscosity conditions, these changes were minimal compared to the fluorescence intensity variations caused by viscosity changes (Figure 6A).

Considering that the cellular matrix is a complex and heterogeneous fluid, fluorescence emission spectra of the probe can be influenced by changes in solvent polarity. Therefore, the fluorescence spectra of **TPE-V1** were investigated in various solvents. It was observed that the probe exhibited high fluorescence emission at 617 nm and 710 nm in 90% glycerol, while displaying extremely weak fluorescence in solvents with different polarities (Figure 6D). Thus, the effect of solvent polarity on the fluorescence intensity of **TPE-V1** can be considered negligible.

To evaluate the specificity of **TPE-V1** for viscosity, its selectivity was examined by adding various ROS, reactive sulfur species (RSS), and metal ions under simulated physiological conditions. Encouragingly, only viscosity led to a significant increase in fluorescence signal at 617 nm and 710 nm, without any interference from other highly reactive ROS, RSS, or metal ions in vivo (Figures 6B-6C, 6E-6F). This demonstrates the excellent selectivity of **TPE-V1** for viscosity measurement.

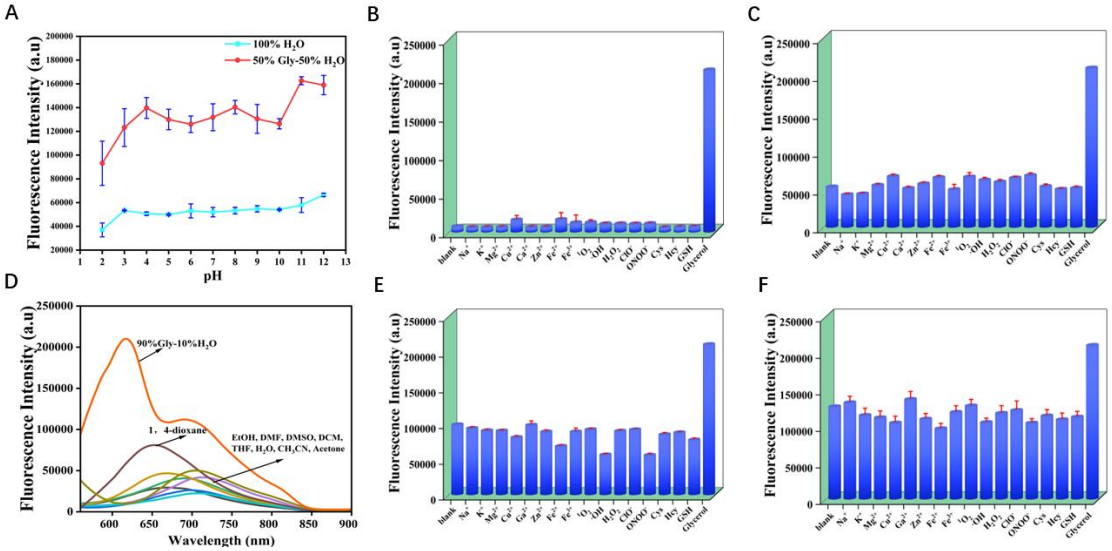

Figure 6. (A) The effect of pH on the fluorescence intensity of **TPE-V1** at high and low viscosities. (D) Emission spectra of **TPE-V1** in various solvents with different

polarities. Fluorescence response of **TPE-V1** (10 μM) to various ROS, RSS and metal ions (200 μM)，which (B) and (E) is at low viscosity (100% H_2O) and high viscosity (50% Gly-50% H_2O), $\lambda_{ex/em}$=540/617 nm, (C) and (F) is at low viscosity (100% H_2O) and high viscosity (50% Gly-50% H_2O), $\lambda_{ex/em}$=540/710 nm.

3.6 Cytotoxicity and co-localization experiments of TPE-V1

Following the characterization of **TPE-V1**'s outstanding photophysical properties, cytotoxicity experiments were conducted to assess its safety for imaging investigations. As illustrated in Figure S9, the cell survival rates remained above 92% for **TPE-V1** concentrations of 0, 5, 10, 25, and 50 μM, indicating the low cytotoxicity of **TPE-V1** for live cell imaging experiments.

To determine the localization of the probe, **TPE-V1** and BODIPY493/503 dyes (the most representative LDs probe) were co-stained in HeLa cells. As shown in Figure 7, a high Pearson coefficient of 0.8806 was obtained by overlapping the spectra from the red and green channels. Additionally, the intensity profiles of **TPE-V1** and BODIPY493/503 for the region of interest (ROI) lines in HeLa cells exhibited synchronous variations. These results collectively demonstrate that light spots mainly represent lipid droplets and **TPE-V1** have a high degree of LDs targeting specificity.

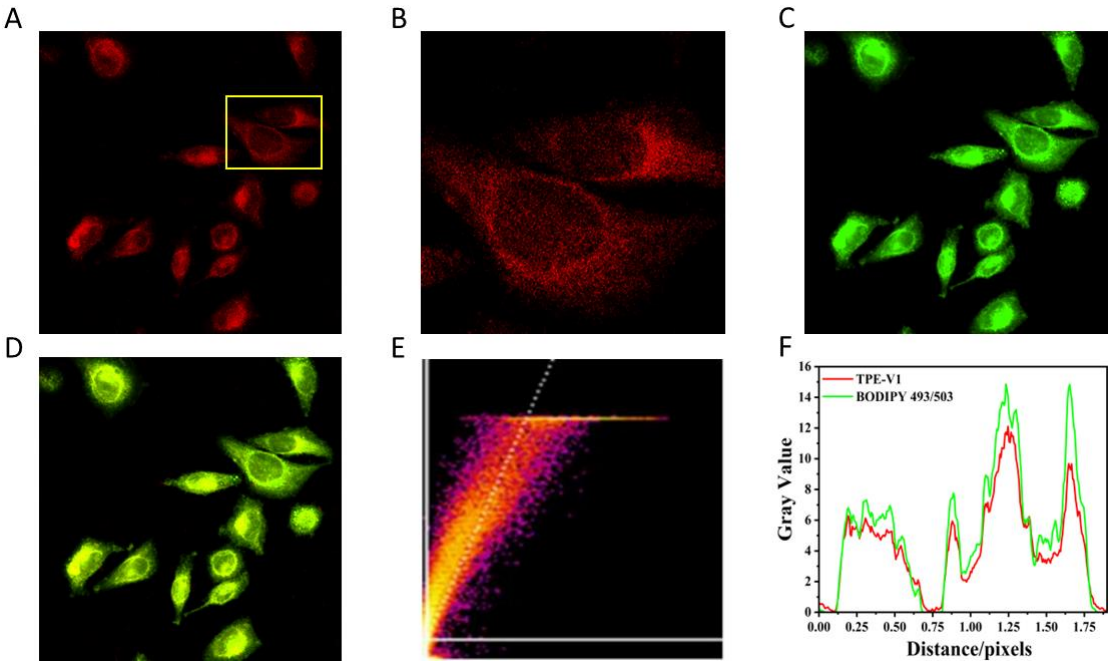

Figure 7. (A, C, D) Confocal fluorescence images of HeLa cells after incubation with

20 μM **TPE-V1** and 10 μM BODIPY493/503 respectively at 37℃ for 10 min. (B) Localized magnification of cells in Figure 7A. (E) The Pearson's correlation coefficient for the overlap between **TPE-V1** and BODIPY493/503. (F) The intensity profile of ROI lines. λ_{ex}=487 nm, λ_{em}=500-550 nm (green channel), λ_{ex}=560 nm, λ_{em}=580-630 nm (red channel). Scale bar=20 μm.

3.7 Viscosity-activated imaging at the cell level

The exceptional cell imaging capability of **TPE-V1** enabled the exploration of its real-time response to viscosity changes in lipid droplets (LDs). Initially, HeLa cells were co-incubated with **TPE-V1** (20 μM) for 10 minutes, followed by treatment with nystatin (10 μM) to induce an increase in intracellular viscosity for an additional 30 minutes. The imaging results were then observed at 5-minute intervals.

As depicted in Figure 8A, the control group treated with PBS (10 μM) exhibited weak fluorescence intensity in both fluorescence channels (λem=580-630 nm, λem=650-750 nm), with no significant changes in fluorescence intensity over time. In contrast, the experimental group demonstrated a strong time-dependent signal enhancement in the red and NIR channels (Figure 8B). To quantitatively describe this relationship, the fluorescence intensity of HeLa cells was plotted as a bar graph against time (Figure 8C and 8D), clearly illustrating the gradual increase in fluorescence intensity in both the red and NIR channels over time. These results conclusively demonstrated that **TPE-V1** enables the analysis and real-time monitoring of mechanical property changes in LDs through the red and NIR channels.

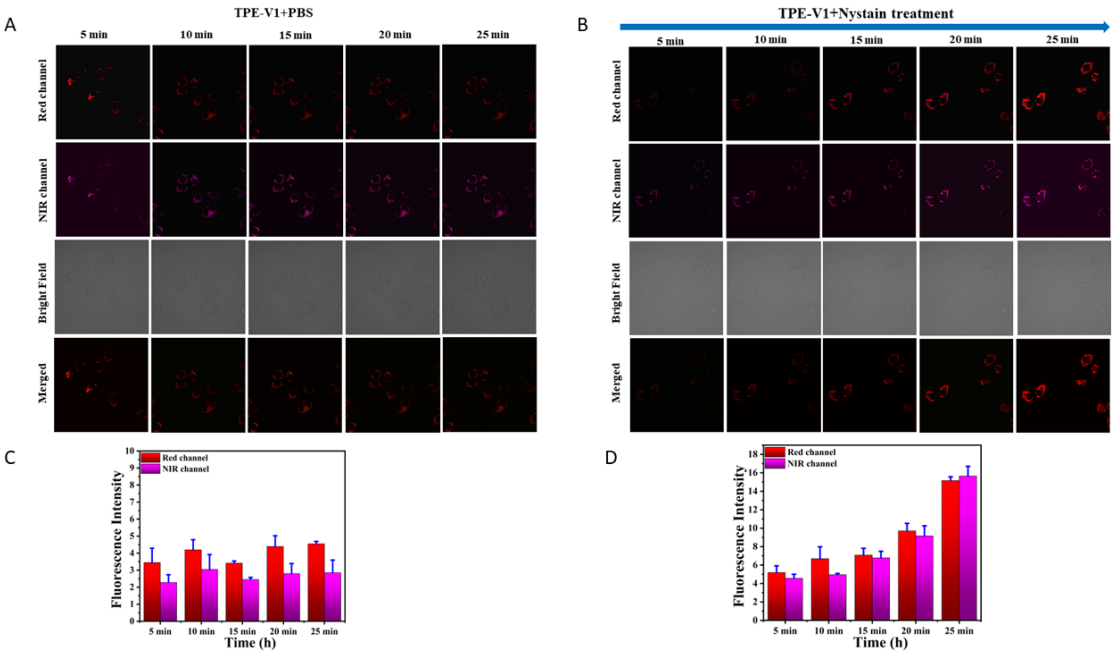

Figure 8. (A) Control group: fluorescence imaging of HeLa cells with 20 μM **TPE-V1**-loaded and 10 μM PBS at 5, 10, 15, 20, and 25 minutes. (B) Experimental group: fluorescence images of HeLa cells with 20 μM **TPE-V1**-loaded and 10 μM nystain at 5, 10, 15, 20, and 25 minutes. (C) Relative fluorescence intensity of control group. (D) Relative fluorescence intensity of experimental group. λ_{ex}=560 nm, λ_{em}=580-630 nm (red channel), λ_{em}=650-750 nm (NIR channel). Scale bar=20 μm.

3.8 Monitoring the viscosity changes of LDs during ferroptosis

Ferroptosis is a distinct form of programmed cell death that differs from apoptosis, cell necrosis, and autophagy. During the ferroptosis process, the accumulation of lipid droplet peroxides and the viscosity of LDs are closely linked [12, 58, 59]. To further comprehend the mechanosensing of LDs viscosity during ferroptosis, HeLa cells were treated with 20 μM **TPE-V1** and 10 μM erastin (a ferroptosis inducer). As depicted in Figure 9A-9B, there was a significant increase in fluorescence intensity in both the red and NIR channels over time. These results clearly demonstrated that ferroptosis accelerated a rapid rise in LDs viscosity, accompanied by morphological changes in the cells indicative of cellular shrinkage and near demise.

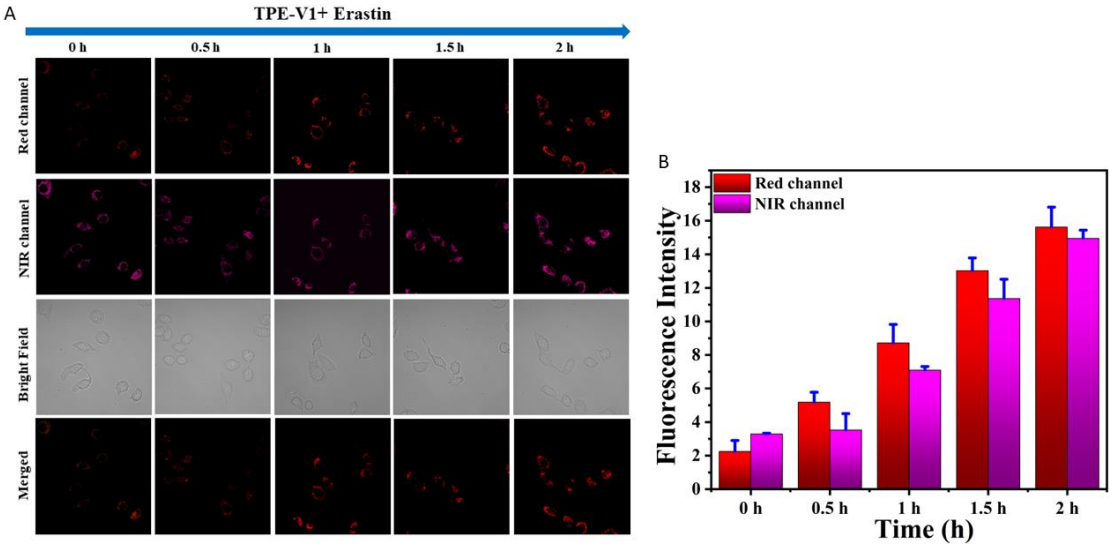

Figure 9. (A) Fluorescence time images of HeLa cells incubated with 20 μM **TPE-V1** for 10 min and 10 μM erastin (0-2 hours). (B) Relative fluorescence intensity at various time (0-2 hours). λ_{ex}=560 nm, λ_{em}=580-630 nm (red channel), λ_{em}=650-750 nm (NIR channel). Scale bar=20 μm.

It is well-known that Ferrostatin 1 (Fer-1) is a widely used inhibitor of ferroptosis that prevents the accumulation of lipid peroxides and the increase in LDs caused by ferroptosis in living cells [16, 60]. To further illustrate the connection between ferroptosis and the increase in LDs viscosity, the variation in viscosity of HeLa cells was investigated by simultaneous incubation with **TPE-V1**, erastin, and Fer-1. At this stage, the fluorescence intensity in the dual channels did not exhibit significant changes over time (Figure S10). These results collectively confirm that enhanced mechanical energy within organelle LDs can trigger biological responses, including cellular mechanosensing (the occurrence of ferroptosis and cellular deformation). This highlights the capability of **TPE-V1** to real-time monitor LDs viscosity using a dual-channel fluorescence-on model during ferroptosis.

4. Conclusion

In conclusion, we successfully designed and synthesized **TPE-V1**, the first fluorescent probe based on the TICT-AIE mechanism, to investigate the mechanical properties (viscosity) of LDs using a dual-channel (red and NIR channels) fluorescence turn-on model. **TPE-V1** demonstrated significant fluorescence enhancement at 617 nm

(red channel) and 710 nm (NIR channel) in high-viscosity media, attributed to the restricted molecular rotation, which effectively inhibited the TICT and AIE processes. The validity of this phenomenon was further supported by theoretical calculations.

By leveraging the long emission wavelength and LDs localization effects, we were able to visualize and analyse the increase in mechanical energy of organelle LDs during the process of ferroptosis through real-time and in situ fluorescence imaging. These findings provide valuable insights into the mechanobiology of organelles during ferroptosis. We anticipate that the utilization of this unique dual-channel fluorescence probe will serve as an effective and accurate method for further investigating the role of organelle mechanobiology in the context of ferroptosis.

Author statement

Ao Yu: Methodology, Data curation, Writing-Original Draft. Wei Zhang: Validation. Qiangsheng Zhang: Validation. Kunlong Yang: Investigation. Xiongbo Liu: Investigation. Hongtao Liu: Investigation. Jialin Xie: Investigation. Yan Feng: Writing-Review & Editing, Visualization. Jianwei Li: Writing-Review & Editing. Chunman Jia: Writing-Review & Editing, Visualization.

Conflicts of interest

There are no conflicts to declare.

Acknowledgments

We are grateful for the financial support from the National Natural Science Foundation of China (22161017, 22161016) and the Start-up Research Foundation of Hainan University (KYQD(ZR)23084, KYQD(ZR)22034).

References

[1] S. Lecoutre, M. Lambert, K. Drygalski, I. Dugail, S. Maqdasy, M. Hautefeuille, et al., Importance of the microenvironment and mechanosensing in adipose tissue biology, Cells, 11(2022) 2310-2338.

[2] H. Zhou, M. Wang, Y. Zhang, Q. Su, Z. Xie, X. Chen, et al., Functions and clinical significance of mechanical tumor microenvironment: cancer cell sensing, mechanobiology and metastasis, Cancer Commun., 42(2022) 374-400.

[3] M. Amer, L. Shi, H. Wolfenson, The 'yin and yang' of cancer cell growth and mechanosensing, Cancers, (13)2021 4754-4774.

[4] W.-J. Fu, J.T. Li, W.H. Qian, X.Y. Zhang, D.D. Ma, Y.T. Wang, et al., Viscosity-triggered near-infrared fluorescence nanoprobe for in vivo non-invasive diagnosis of cancer, Chem. Eng. J., 464(2023) 142521.

[5] Z. Yan, G. Su, W. Gao, J. He, Y. Shen, Y. Zeng, et al., Fluid shear stress induces cell migration and invasion via activating autophagy in HepG2 cells, Cell Adhes. Migr., 13(2019) 152-163.

[6] H.J. Lee, M.F. Diaz, K.M. Price, J.A. Ozuna, S. Zhang, E.M. Sevick-Muraca, et al., Fluid shear stress activates YAP1 to promote cancer cell motility, Nat. Commun., 8(2017) 14122.

[7] S. Ma, A. Fu, G.G.Y. Chiew, K.Q. Luo, Hemodynamic shear stress stimulates migration and extravasation of tumor cells by elevating cellular oxidative level, Cancer Lett., 388(2017) 239-248.

[8] Scott J. Dixon, Kathryn M. Lemberg, Michael R. Lamprecht, R. Skouta, Eleina M. Zaitsev, Caroline E. Gleason, et al., Ferroptosis: An iron-dependent form of nonapoptotic cell death, Cell, 149(2012) 1060-1072.

[9] R. Lin, Z. Zhang, L. Chen, Y. Zhou, P. Zou, C. Feng, et al., Dihydroartemisinin (DHA) induces ferroptosis and causes cell cycle arrest in head and neck carcinoma cells, Cancer Lett., 381(2016) 165-175.

[10] L. Chen, W.S. Hambright, R. Na, Q. Ran, Ablation of the ferroptosis inhibitor glutathione peroxidase 4 in neurons results in rapid motor neuron degeneration and paralysis*, J. Biol. Chem, 290(2015) 28097-28106.

[11] S.J. Guiney, P.A. Adlard, A.I. Bush, D.I. Finkelstein, S. Ayton, Ferroptosis and cell death mechanisms in Parkinson's disease, Neurochem. Int., 104(2017) 34-48.

[12] B.R. Stockwell, J.P. Friedmann Angeli, H. Bayir, A.I. Bush, M. Conrad, S.J. Dixon, et al., Ferroptosis: a regulated cell death nexus linking metabolism, redox biology, and disease, Cell, 171(2017) 273-285.

[13] W.S. Yang, B.R. Stockwell, Synthetic lethal screening identifies compounds activating iron-dependent, nonapoptotic cell death in oncogenic-RAS-harboring cancer cells, Chem. Biol, 15(2008) 234-245.

[14] N. Yagoda, M. von Rechenberg, E. Zaganjor, A.J. Bauer, W.S. Yang, D.J. Fridman, et al., RAS-RAF-MEK-dependent oxidative cell death involving voltage-dependent anion channels, Nature, 447(2007) 865-869.

[15] Wan S. Yang, R. SriRamaratnam, Matthew E. Welsch, K. Shimada, R. Skouta, Vasanthi S. Viswanathan, et al., Regulation of ferroptotic cancer cell death by GPX4, Cell, 156(2014) 317-331.

[16] B. Dong, W. Song, Y. Lu, Y. Sun, W. Lin, Revealing the viscosity changes in lipid droplets during ferroptosis by the real-time and in situ near-infrared imaging, ACS Sens, 6(2021) 22-26.

[17] Y. Zou, M.J. Palte, A.A. Deik, H. Li, J.K. Eaton, W. Wang, et al., A GPX4-dependent cancer cell state underlies the clear-cell morphology and confers sensitivity to ferroptosis, Nat. Commun., 10(2019) 1617.

[18] Y. Bai, L. Meng, L. Han, Y. Jia, Y. Zhao, H. Gao, et al., Lipid storage and lipophagy regulates

ferroptosis, Biochem. Biophys. Res. Commun., 508(2019) 997-1003.
[19] R. Chen, Z. Li, C. Peng, L. Wen, L. Xiao, Y. Li, Rational design of novel lipophilic aggregation-induced emission probes for revealing the dynamics of lipid droplets during lipophagy and ferroptosis, Anal. Chem., 94(2022) 13432-13439.
[20] G. Liu, H. Zheng, J. Dai, H. Li, R. Zhou, C. Wang, et al., Long-term in-situ real-time fluorescence imaging of lipid droplets during cell ferroptosis process enabled by an epindolidione-based fluorescent probe, Sens. Actuators, B, 381(2023) 133438.
[21] J. Yin, J. Zhan, Q. Hu, S. Huang, W. Lin, Fluorescent probes for ferroptosis bioimaging: advances, challenges, and prospects, Chem. Soc. Rev., 52(2023) 2011-2030.
[22] J.W. Dufty, Fourier's law for a granular fluid, J. Phys. Chem. C, 111(2007) 15605-15612.
[23] Y. Deng, G. Feng, Visualization of $ONOO^-$ and viscosity in drug-induced hepatotoxicity with different fluorescence signals by a sensitive fluorescent probe, Anal. Chem., 92(2020) 14667-14675.
[24] S. Wang, B. Zhou, N. Wang, C. Yu, N. Yang, J. Chen, et al., Mitochondria-targeted fluorescent probe based on vibration-induced emission for real-time monitoring mitophagy-specific viscosity dynamic, Chin Chem Lett, 31(2020) 2897-2902.
[25] M.A. Haidekker, T.P. Brady, D. Lichlyter, E.A. Theodorakis, A ratiometric fluorescent viscosity sensor, J. Am. Chem. Soc, 128(2006) 398-399.
[26] A. Jiménez-Sánchez, E.K. Lei, S.O. Kelley, A multifunctional chemical probe for the measurement of local micropolarity and microviscosity in mitochondria, Angew. Chem. Int. Ed., 57(2018) 8891-8895.
[27] X. Wu, G. Fu, Y. Li, S. Li, Q. Zhao, F. Kong, et al., Dihydroxanthene-based near-infrared fluorescent probes for monitoring mitochondrial viscosity in living cells and mice, Anal. Chem., 95(2023) 3544-3549.
[28] W. Pan, L. Han, X. Cao, S. Shen, X. Pang, Y. Zhu, Dual-response near-infrared fluorescent probe for detecting cyanide and mitochondrial viscosity and its application in bioimaging, Food Chem, 407(2023) 135163.
[29] C. Liu, T. Zhao, S. He, L. Zhao, X. Zeng, A lysosome-targeting viscosity-sensitive fluorescent probe based on a novel functionalised near-infrared xanthene-indolium dye and its application in living cells, J. Mater. Chem. B, 8(2020) 8838-8844.
[30] L. Dai, M. Ren, Z. Li, L. Wang, W. Lin, A targetable fluorescent probe for imaging of mitochondrial viscosity in living cells, Anal. Methods, 11(2019) 4561-4565.
[31] Y. Zhang, A. Qin, S. Gong, M. Li, Z. Meng, Y. Liang, et al., Two birds with one stone: A novel dual-functional fluorescent probe for simultaneous monitoring and real-time imaging of alkaline pH and viscosity in living cells, Microchem. J., 173(2022) 107010.
[32] T. Guo, X. Chen, W. Qu, B. Yang, R. Tian, Z. Geng, et al., Red and near-infrared fluorescent probe for distinguishing cysteine and homocysteine through single-wavelength excitation with distinctly dual emissions, Anal. Chem., 94(2022) 5006-5013.
[33] Y. Hontani, F. Xia, C. Xu, Multicolor three-photon fluorescence imaging with single-wavelength excitation deep in mouse brain, Sci. Adv, 7(2021) eabf3531.
[34] S.A. Hilderbrand, R. Weissleder, Near-infrared fluorescence: application to in vivo molecular imaging, Curr. Opin. Chem. Biol., 14(2010) 71-79.
[35] L. Yuan, W. Lin, K. Zheng, L. He, W. Huang, Far-red to near infrared analyte-responsive fluorescent probes based on organic fluorophore platforms for fluorescence imaging, Chem. Soc. Rev., 42(2013) 622-661.
[36] M. Kang, Z. Zhang, N. Song, M. Li, P. Sun, X. Chen, et al., Aggregation-enhanced theranostics:

AIE sparkles in biomedical field, Aggregate, 1(2020) 80-106.
[37] Z. Guo, C. Yan, W.-H. Zhu, High-performance quinoline-malononitrile core as a building block for the diversity-oriented synthesis of AIEgens, Angew. Chem. Int. Ed., 59(2020) 9812-9825.
[38] J.-J. Hu, W. Jiang, L. Yuan, C. Duan, Q. Yuan, Z. Long, et al., Recent advances in stimuli-responsive theranostic systems with aggregation-induced emission characteristics, Aggregate, 2(2021) 48-65.
[39] W.-J. Shi, X.-H. Yan, J. Yang, Y.-F. Wei, Y.-T. Huo, C.-L. Su, et al., Development of meso-five-membered heterocycle BODIPY-based AIE fluorescent probes for dual-organelle viscosity imaging, Anal. Chem., 95(2023) 9646-9653.
[40] J. Ge, W. Cai, N. Niu, Y. Wen, Q. Wu, L. Wang, et al., Viscosity-responsive NIR-II fluorescent probe with aggregation-induced emission features for early diagnosis of liver injury, Biomaterials, 300(2023) 122190.
[41] Y. Zhang, Z. Li, W. Hu, Z. Liu, A mitochondrial-targeting near-infrared fluorescent probe for visualizing and monitoring viscosity in live cells and tissues, Anal. Chem., 91(2019) 10302-10309.
[42] B. Chen, C. Li, J. Zhang, J. Kan, T. Jiang, J. Zhou, et al., Sensing and imaging of mitochondrial viscosity in living cells using a red fluorescent probe with a long lifetime, Chem. Commun., 55(2019) 7410-7413.
[43] T. Chen, Z. Chen, R. Liu, S. Zheng, A NIR fluorescent probe for detection of viscosity and lysosome imaging in live cells, Org. Biomol. Chem., 17(2019) 6398-6403.
[44] S.-J. Li, Y.-F. Li, H.-W. Liu, D.-Y. Zhou, W.-L. Jiang, J. Ou-Yang, et al., A dual-response fluorescent probe for the detection of viscosity and H_2S and its application in studying their cross-talk influence in mitochondria, Anal. Chem., 90(2018) 9418-9425.
[45] Y. Wu, C. Yin, W. Zhang, Y. Zhang, F. Huo, Mitochondrial-targeting near-infrared fluorescent probe for visualizing viscosity in drug-induced cells and a fatty liver mouse model, Anal. Chem., 94(2022) 5069-5074.
[46] M. Zhang, J. Li, L. Yu, X. Wang, M. Bai, Tuning the fluorescence based on the combination of TICT and AIE emission of a tetraphenylethylene with D–π–A structure, RSC Adv., 10(2020) 14520-14524.
[47] Q. Hu, Q. Huang, K. Liang, Y. Wang, Y. Mao, Q. Yin, et al., An AIE+TICT activated colorimetric and ratiometric fluorescent sensor for portable, rapid, and selective detection of phosgene, Dyes Pigm., 176(2020) 108229.
[48] J.-h. Zhu, H. Zhang, Y. Liao, J.-j. Liu, Z.-j. Quan, X.-c. Wang, A multifunctional fluorescent probe for highly selective detection of hydrazine and discovering the interplay between AIE and ICT, Dyes Pigm., 175(2020) 108111.
[49] Y.-C. Chiang, Z.-L. Lai, C.-M. Chen, C.-C. Chang, B. Liu, Construction of emission-tunable nanoparticles based on a TICT-AIEgen: impact of aggregation-induced emission versus twisted intramolecular charge transfer, J. Mater. Chem. B, 6(2018) 2869-2876.
[50] R. Hu, E. Lager, A. Aguilar-Aguilar, J. Liu, J.W.Y. Lam, H.H.Y. Sung, et al., Twisted intramolecular charge transfer and aggregation-induced emission of BODIPY derivatives, J. Phys. Chem. C, 113(2009) 15845-15853.
[51] S. Zhu, R. Tian, A.L. Antaris, X. Chen, H. Dai, Near-infrared-II molecular dyes for cancer imaging and surgery, Adv. Mater., 31(2019) 1900321.
[52] B. Li, M. Zhao, F. Zhang, Rational design of near-infrared-II organic molecular dyes for bioimaging and biosensing, ACS Mater. Lett., 2(2020) 905-917.
[53] E. Wang, E. Zhao, Y. Hong, J.W.Y. Lam, B.Z. Tang, A highly selective AIE fluorogen for lipid droplet imaging in live cells and green algae, J. Mater. Chem. B, 2(2014) 2013-2019.

[54] F. Wu, Y. Lu, X. Mu, Z. Chen, S. Liu, X. Zhou, et al., Intriguing H-Aggregates of heptamethine cyanine for imaging-guided photothermal cancer therapy, ACS Appl. Mater. Interfaces, 12(2020) 32388-32396.
[55] S. Liu, X. Zhou, H. Zhang, H. Ou, J.W.Y. Lam, Y. Liu, et al., Molecular motion in aggregates: manipulating TICT for boosting photothermal theranostics, J. Am. Chem. Soc., 141(2019) 5359-5368.
[56] S. Liu, Y. Li, R.T.K. Kwok, J.W.Y. Lam, B.Z. Tang, Structural and process controls of AIEgens for NIR-II theranostics, Chem. Sci, 12(2021) 3427-3436.
[57] H. Zhang, Z. Zhao, A.T. Turley, L. Wang, P.R. McGonigal, Y. Tu, et al., Aggregate science: from structures to properties, Adv. Mater. 32(2020) 2001457.
[58] H. Li, W. Shi, X. Li, Y. Hu, Y. Fang, H. Ma, Ferroptosis accompanied by •OH generation and cytoplasmic viscosity increase revealed via dual-functional fluorescence probe, J. Am. Chem. Soc., 141(2019) 18301-18307.
[59] K.-N. Wang, L.-Y. Liu, D. Mao, S. Xu, C.-P. Tan, Q. Cao, et al., A polarity-sensitive ratiometric fluorescence probe for monitoring changes in lipid droplets and nucleus during ferroptosis, Angew. Chem., Int. Ed., 60(2021) 15095-15100.
[60] O. Zilka, R. Shah, B. Li, J.P. Friedmann Angeli, M. Griesser, M. Conrad, et al., On the mechanism of cytoprotection by ferrostatin-1 and liproxstatin-1 and the role of lipid peroxidation in ferroptotic cell death, ACS Cent. Sci., 3(2017) 232-243.